UNIVERSITY OF PITTSBURGH

ORTHOPAEDIC ROBOTICS LABORATORY

2014 SUMMER UNDERGRADUATE ABSTRACT BOOKLET

PITT | SWANSON ENGINEERING
BIOENGINEERING

FOREWARD

The Orthopaedic Robotics Laboratory is the University of Pittsburgh's newly formed collaborative effort between the Department of Bioengineering and Department of Orthopaedic Surgery. The mission of the ORL is the prevention of degenerative joint diseases by improving diagnostic, repair, and rehabilitation procedures for musculoskeletal injuries using state-of-the-art robotic technology. The ORL would like to commend the work of the undergraduate students during the summer of 2014. Students made significant impacts in the study of hand, shoulder, knee, and spinal degenerative joint diseases. The work of our students, with the help of our mentors, contributes greatly to world of Orthopaedic Research and to all patients who benefit.

OUR TEAM

Kyle Berkow
Class of 2016
Bioengineering
University of Pittsburgh

Ryan Moss
Class of 2015
Bioengineering
University of Pittsburgh

Stephanie Rigot
Class of 2015
Bioengineering
University of Rochester

Yaniv Michaeli
Class of 2015
Mechanical Engineering
Braude College of Engineering, Israel

Gerald Ferrar
Class of 2015
Bioengineering
University of Pittsburgh

Benjamin Engel
Class of 2015
Bioengineering
University of Pittsburgh

TABLE OF CONTENTS

1. **Validation of Patellofemoral Joint Contact Pressure Distribution Driven by Accurate Knee Joint Kinematics** — **Page 5-7**
   Kyle Berkow, Jonathan Gustafson, Zhaochun Yang, Richard Debski, PhD, Shawn Farrokhi, PhD, DPT
   Department of Bioengineering and Department of Physical Therapy

2. **Biomechanical Analysis of Internal Fixation Methods for Distal Interphalangeal Joint Arthrodesis** — **Page 8-9**
   Stephanie Rigot, Rafael Diaz-Garcia, MD, Richard Debski, PhD, John Fowler, MD
   Department of Bioengineerng and Department of Orthopaedic Surgery

3. **Effect of Tear Chronicity on Rotator Cuff Tendon Tear Propagation** — **Page 10-11**
   Gerald Ferrer, Mathew Miller, Volker Musahl, MD, Richard Debski, PhD
   Department of Bioengineering and Department of Orthopaedic Surgery

4. **Effects of Anterolateral Capsular Injury and Extra-Articular Tenodesis on Knee Kinematics During Physical Examination** — **Page 12-14**
   Benjamin Engel, Fabio Arilla, MD, Ata Azar, MD, Daniel Guenther, MD, Carlos Yacuzzi, MD, Richard Debski, PhD, Volker Musahl, MD
   Department of Bioengineering and Department of Orthopaedic Surgery

5. **A New Method for Determining Cross-Sectional Shape and Area of Soft Tissues Using 3D Laser Scanning** — **Page 15-17**
   Yaniv Michaeli, Richard Debski, PhD
   Department of Bioengineering

6. **The Effect of Various Loading Conditions of 3D Cervical Spine** — **Page 18-19**
   Ryan Moss, Kevin Bell, PhD
   Department of Bioengineering

Validation of Patellofemoral Joint Contact Pressure Distribution Driven by Accurate Knee Joint Kinematics

Berkow, KA.; Gustafson, J A.; Yang, Z; Debski, RE.; Farrokhi, S
Departments of Bioengineering and Physical Therapy, University of Pittsburgh, Pittsburgh, PA

Introducion: Patellofemoral Pain Syndrome (PFPS) accounts for 25-40% of knee problems presenting in sports medicine centers and has been linked to early onset of osteoarthritis development. [1, 2] A commonly proposed mechanism for development of pain is increased contact pressure at the cartilage surfaces and subchondral bone caused by maltracking of the patella as a result of excessive rotations of the femur. [3, 4] Limitations measuring in vivo contact pressure require the use of computational models. Accurate, in vivo kinematics could be used to drive these computational models and predict joint contact pressure during functional tasks to aid in diagnosing patients with PFPS and evaluating the effectiveness of rehabilitative treatments. However, it is necessary that these computational models are validated prior to implementation in vivo. The objective of this work was to compare patellofemoral contact pressure distribution between in vitro experimental data and computational models employing the discrete element analysis (DEA) technique driven by kinematics collected experimentally. We hypothesized that contact area and average contact pressure between the experimental data and DEA model would be similar and that increased femoral rotation would correlate with increased contact pressure.

Method: Inputs to the computational model included knee geometry, cartilage material properties, and experimental kinematics while experimental contact pressures served as validation data. A fresh-frozen cadaveric knee was initially prepared by: 1) isolation of the quadriceps tendons, 2) affixing rigid registration blocks to the femur, patella and tibia for digitization, and 3) acquiring high resolution MRI scans of the extended, unloaded knee. Model geometry of the knee was developed from manual segmentation (Mimics®, Materialise, Leuven, Belgium) of bone, cartilage, and registration blocks from the MRI scans. Surface geometry was created from the segmentation process and imported into meshing software (Hypermesh, Altair Engineering Inc., Troy, MI). Tetrahedral, shell elements with an average element size of 2 mm were used to model the bones and cartilage.

Experimentally, a six degree of freedom knee jig was used to apply physiologic compressive loading to the tibiofemoral joint and tensile loading to the quadriceps tendon [5] at 15 degrees of tibiofemoral flexion (representing the loading response phase of gait) with the femur in three positions: 1) neutral alignment, 2) internal rotation of 5 degrees, and 3) external rotation of 5 degrees. Kinematic data was collected at each position using a mechanical digitizer (Faro Arm®, Lake Mary, FL). Patellofemoral pressure distributions were recorded at each position by performing a lateral retinacular release in order to insert a calibrated thin, flexible pressure sensor (K-scan Model 5051, 2.5K psi; Tekscan Inc., South Boston, MA).

DEA was utilized for computational analysis at each position by creating compression-only springs ($E=4MPa$, $\nu=0.45$ [6]) at the centroid of each element of the segmented femoral and patellar cartilage surfaces. Local coordinate systems built on the surface of the registration blocks were used to relate the position of the knee model from the MRI scans to each of the experimental positions in order to load the joint. [7] Contact pressure distributions were estimated based on the deformation of the springs and divided into medial and lateral facet

regions for analysis. Validation was performed by comparing the percent error of contact area and average pressure between the computational model and experimental data collected for each region. A Pearson's r correlation analysis was performed to quantify the relationship between average joint contact pressure and femoral rotation.

Results: Qualitatively, the contact patterns between the computational model and experimental data were similar and changed with femoral rotation (**Figure 1**). The largest difference in contact area between the DEA analysis and experimental data occurred on the lateral facet in 5 degrees of internal rotation (Error = 25%). The largest error in average contact pressure occurred on the medial facet in neutral (Error = 46%). A strong correlation of contact pressure with femoral rotation existed that showed an increase in average contact pressure on the lateral facet from an externally rotated femur to an internally rotated femur (Experimental: r = 0.99; Computational: r = 0.93). There were also strong correlations of a decrease in average contact pressure on the medial facet from an externally rotated femur to an internally rotated femur (Experimental: r = -0.95). The contact pressure at 5 degrees of internal rotation was below the minimum threshold set by the computational model (10 KPa) and was not calculated.

Table 1. Patellofemoral contact variables between experimental and computational results for the three femoral positions at 15° of flexion

		Lateral Facet			**Medial Facet**		
		ER = 5°	**Neutral**	**IR = 5°**	**ER = 5°**	**Neutral**	**IR = 5°**
Experimental Results	Contact Area (mm^2)	198	211	194	150	111	37
Computational Results	Contact Area (mm^2)	170	196	242	171	102	0
Experimental Results	Average Contact Pressure (KPa)	214	281	376	197	156	145
Computational Results	Average Contact Pressure (KPa)	292	302	364	146	84	0

Discussion: This study examined the validity of creating DEA models driven by kinematic data and estimating contact pressure distribution at the patellofemoral joint. The computational experimental data collected. An important finding from this study is the models ability to distinguish between femoral rotation positions. The maximum contact pressure occurred on the lateral facet at 5 degrees of femoral internal rotation with a trend of increasing pressure from an externally rotated femur to an internally rotated femur. A decrease in pressure on the lateral facet was observed at 5 degrees of external rotation for the experimental data and computational model. These results are similar to those from a previous study [4], indicating that femoral motion has a significant impact on patellofemoral joint contact pressure. Differences between the computational model and experimental data could be due to the number and size of the springs utilized for the DEA analysis, material properties of the springs, as well as a minimum threshold of 10 KPa used to determine contact that may have missed regions of contact. In the future, a sensitivity analysis will be performed to examine the effect of the input parameters on the contact pressure and additional computational models will be validated. Ultimately, our goal is to use these validated computational models with accurate 3D joint kinematics to estimate joint contact pressures during dynamic activities in vivo.

model showed good agreement in terms of contact area and average pressure compared to the

Significance: The results of this study demonstrate changes in patellofemoral contact patterns with varying degrees of femoral rotation in a computational model. By validating these computational models, it may be possible to utilize accurate kinematic data collection methods to better predict in vivo patellofemoral cartilage pressures throughout different dynamic activities, potentially aiding in development of appropriate therapeutic treatment programs for patients with PFPS.

Acknowledgements: The project described was supported by the National Institutes of Health (K12 HD055931) and the Pittsburgh Claude D. Pepper Older Americans Independence Center (P30 AG024827).

References: [1] DeHaven K. Am J Sports Med, 1986. [2] Thomée R. Sports Med. 1999. [3] Fulkerson, JP. J Bone Joint Surg Am, 1990. [4] Lee, TQ. Clin Orthop Relat R, 1994. [5] Hofer J. J Arthroplasty, 2012. [6] Blankevoort L. J Biomech Eng, 1991. [7] Fischer KJ. J Biomech, 2001.

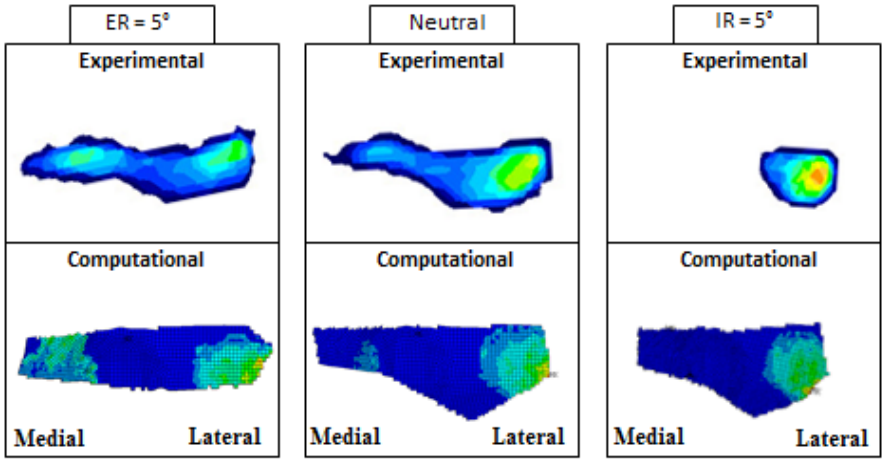

Figure 1: Patellofemoral contact pressure distributions between experimental and computational results for the three femoral positions at 15° flexion (IR/ER = Internal/External rotation)

Biomechanical Analysis of Internal Fixation Methods for Distal Interphalangeal Joint Arthrodesis

Rigot, S [1,2]; Diaz-Garcia, R [2,4]; Debski, RE [2,3,4]; Fowler, J [2,4]

1. Department of Biomedical Engineering, University of Rochester, Rochester, NY, United States.
2. Orthopaedic Robotics Laboratory, University of Pittsburgh, Pittsburgh, PA, United States.
3. Department of Bioengineering, University of Pittsburgh, Pittsburgh, PA, United States.
4. Department of Orthopaedic Surgery, University of Pittsburgh, Pittsburgh, PA, United States.

Introduction: Arthrodesis is a common procedure used to treat pain, deformity, or instability of the distal interphalangeal (DIP) joint [1]. Many techniques are clinically accepted to achieve arthrodesis of the DIP joint in the hand and have typically been evaluated during load-to-failure tests [2, 3]. However, cyclic loading can occur from daily use of the finger in the 6-8 weeks after surgery that may disrupt the ability of the joint to achieve a stable arthrodesis. Therefore, the objective of this study is to assess the biomechanical performance of 4 DIP fixation techniques in response to cyclic and load-to-failure bending loads.

Methods: Twenty-eight (n=7 for each of the 4 fixation methods) fresh, frozen cadaveric distal and middle phalanx pairs from the index, middle, and ring fingers were fixed by one of the following techniques (Figure 1): 1) two parallel 0.045" Kirschner wires ('parallel K-wires'), 2) one longitudinal 0.045" K-wire and one oblique 0.045" K-wire ('crossed K-wires'), 3) a 24mm Acutrak 2 Micro headless compression screw ('screw'), or 4) 27-gauge dental wire loops in the medial-lateral and proximal-distal directions across the DIP joint ('dental wire'). The fixations were all performed by a fellowship-trained hand surgeon following standardized methodologies. The phalanx was then loaded in a cantilever cyclic loading test with a 10N maximum force for 3,000 cycles. The force was applied to the palmar side of the distal phalanx with the force [4] and number of cycles comparable to the normal expected usage in a post-surgery phalanx during the 6-8 week time period before bony fusion generally occurs. The gap size between the distal and middle phalanx in the DIP joint ('DIP gap size') was measured with digital calipers before and after cycling on the palmar side of the phalanges. The bending stiffness was calculated on the first and last cycles of the cyclic loading and the plastic deformation was recorded after the cyclic loading. After cycling, the phalanx was loaded to failure to determine the strength of the fixation method. The maximum bending load and the maximum deflection of the phalanx at failure were recorded. One-way analysis of variance (ANOVA) and Tukey's honestly significant difference test were performed to assess differences between the fixation methods. Significance was set at $p<0.05$.

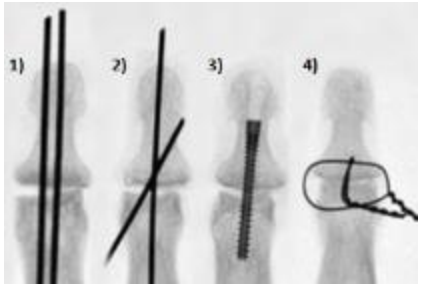

Figure 1: Fluoroscopic images of the fixation methods from the Anterior-Posterior View. 1) Parallel K-wires, 2) Crossed K-wires, 3) Screw, 4) Dental Wire

Results: The dental wire was significantly different from the other 3 fixation techniques in the initial bending stiffness ($p<0.000$), as the initial bending stiffness was approximately 40% of the initial bending stiffness of the screw (Table 1). The amount of plastic deformation ($p<0.000$) and the change in the DIP gap size

(p<0.000) for the dental wire were both significantly different from the other methods and were about 10 and 15 times larger in deformation and gap size than the other methods, respectively. The dental wire had a maximum deflection at failure ~2.6 times larger than that of the screw (p<0.000) and both the screw and dental wire were significantly different from the other methods in the maximum bending load at failure (p<0.000).

Discussion: The significant differences due to the cyclic loading suggest that the dental wire technique would undergo more motion at the arthrodesis site during everyday use than the other three techniques, possibly leading to decreased fusion rates. Specifically, the significantly larger increase in the DIP gap size would likely reduce the compression in the joint which is suggested to slow or decrease the fusion rates [5]. The crossed K-wires, parallel K-wires, and screw produced similar results, suggesting that any of these methods may be suitable for DIP arthrodesis. Our data supports clinical outcome studies showing similar non-fusion rates among headless compression screws and K-wire techniques [1, 6]. Other factors, such as cost and complications, would need to be considered to determine the best fixation method for a particular patient.

Significance: The results of this study will provide useful information to both surgeons and patients that will assist them in choosing the optimal fixation method by considering the biomechanical performance of the fixation, costs, and complications. The dental wire may not be as suitable of an option as the crossed K-wires, parallel K-wires, or compression screw for DIP arthrodesis.

References: [1] Brutus JP et al. J of Hand Surg Am. 2006; 31(1): 85-89. [2] Kovach JC et al. J Hand Surg Am. 1986; 11(4): 562-566. [3] Wyrsch B et al. J Hand Surg Am. 1996; 21(3): 438-443. [4] Smaby N et al. J Rehabil Res Dev. 2004; 41(2): 215-24. [5] Konan S et al.Acta Orthop Belg. 2013; 79(2): 154-158. [6] Engel J et al. Plast Reconstr Surg. 1977; 60(4):611-614.

	1st to Last Cycle Changes (Δ)			Load to Failure	
Fixation Technique	Initial Bending Stiffness (N/mm)	Plastic Deformation (mm)	Δ DIP Gap Size (mm)	Maximum Deflection (mm)	Maximum Bending Load (N)
Dental Wire	5.12 ± 1.44 *	6.24 ± 1.11 *	1.52 ± 0.48 *	12.0 ± 1.38 *	19.7 ± 3.90 *
Crossed K-Wires	9.82 ± 2.02	0.66 ± 0.16	0.25 ± 0.17	5.42 ± 1.00	33.8 ± 2.34
Parallel K-Wires	10.6 ± 2.66	0.66 ± 0.25	0.10 ± 0.05	5.07 ± 1.24	37.4 ± 6.03
Screw	13.1 ± 3.65	0.64 ± 0.44	0.10 ± 0.08	4.67 ± 1.72	45.2 ± 6.90 *

Table 1: Parameters representing the biomechanical performance of the four methods during the cyclic loading and load to failure tests (mean ± SD; * p<0.05).

Effect of Tear Chronicity on Rotator Cuff Tendon Tear Propagation

Ferrer, GA[1]; Miller, RM[1]; Musahl, V[2,1] Debski, RE[1,2]

1. Department of Bioengineering, University of Pittsburgh, Pittsburgh, PA, United States.
2. Department of Orthopaedic Surgery, University of Pittsburgh, Pittsburgh, PA, United States.

Introduction: Rotator cuff tears are a significant clinical problem, with increased age leading to a higher prevalence of chronic rotator cuff tears [1, 2]. The increased age also leads to worse surgical outcomes and increased fatty degeneration, with chronic tears known for having significant tendon degeneration [3, 4]. However, little is known about the differences in tear propagation for acute and chronic tears. Previous studies have used surgically-created acute tears to investigate effects of tear propagation, which do not account for tissue degeneration associated with chronic tears [5]. Therefore, the objective of the study is to characterize tear propagation in shoulders with pre-existing, chronic tears during tensile cyclic loading. It was hypothesized that chronic degenerative tears would propagate at lower loads than acute tears.

Methods: Five fresh frozen cadaveric shoulder specimens (age 64 ± 10 years) with chronic rotator cuff tears were dissected to remove all soft tissue except for the supraspinatus, infraspinatus, and subscapularis tendons. Specimens were grouped based on the AP tear size and amount of retraction at 90 degrees of adbduction (Small/Medium: < 3 cm, Large: 3 – 5 cm, Massive: > 5 cm) [6]. The distance from the LHBT measurements were also made with a digital caliper. The diaphysis of each humerus was potted in epoxy putty and secured to the base of a materials testing machine (Instron, Model 5965). The supraspinatus tendon was secured to the crosshead for uniaxial tensile loading during 90° of coronal-plane abduction. A static 22 N load was placed on the infraspinatus via a pulley system to mimic in vivo load interaction between the infraspinatus and supraspinatus tendons (Figure 1). A 10N preload was applied to the supraspinatus, then preconditioned from 10-25N at 20 mm/min for 100 cycles. After preconditioning, the max load was then increased to 50N for 100 cycles. This was followed by additional loading sets of 100 cycles and 50N max load increase. Cyclic loading continued until a critical tear retraction was reached (100% increase of ML tear size for small/medium sized tears, 50% increase for large, and 25% increase for massive tears) or tendon failure. Additionally, the stiffness for the second cycle of each loading set was determined for the tendon. Correlations between tear size and the load at critical tear retraction were made. Correlations between tear size and stiffness were also made. Significance was set at $p < 0.05$.

Results: The AP tear size for large group was 96% larger than the small/medium group, and the massive group was 40% larger than the large group (Table 1). The ML retraction size for the large group was 104% larger than the small/medium group, and the massive group 74% bigger than the large group (Table 1). As the tear size increased, the tear extended farther anteriorly, closer and even past the LHBT (Table 1). There was a trend that as tear size increased, stiffness would decrease, but no correlation could be found (Table 1) ($p > 0.05$). The load at critical tear retraction was highest for the large tears, and lowest for massive tears (Table 1). No correlation between tear size and load at critical tear retraction could be found ($p > 0.05$). Regardless of the size of the chronic rotator cuff tear, the average load and cycles completed to reach an end of test criteria was 425 ± 86 N. For all chronic tears tested, the

average number of cycles completed before reaching the end of the test was 855 ± 185 cycles. Four of the five tendons failed at the tendon midsubstance while the other failed at the anterior tendon insertion site.

Discussion: This study examined the effects of tear chronicity on tear propagation through cyclic loading to critical tear retraction or tendon failure. The results of this study show that the load at critical tear retraction for chronic tears was about 200-300N less than in acute tears [5]. Despite the degenerative nature of the tissue, tendons with chronic tears are still tough, evident from the number of cycles completed. When comparing the stiffness at the largest common load for each group (300 N), though not significant, tendons were most stiff for small/medium sized tears, and least stiff for the massive tears. Additionally, even though the retraction size increased for all tests, no major signs of tear propagation existed. However, the results do show a trend that as tear size increases, the strength decreases. Therefore, the abnormal firing of muscles which cause different load distributions, or subacromial impingement may be more important factors than tear chronicity when considering what affects tear propagation. In the current study, there was a small sample size for larger chronic tears and tendon degeneration was not quantified. In the future, histology will be performed to quantify the degeneration in the tendons, and finite element models will be created to investigate the effects of the various shapes and sizes for chronic rotator cuff tears on tear propagation.

Significance: Knowing that chronic tears do not propagate at lower loads than acute tears will provide better insight on surgical timing and technique. The results of this study show that it is not essential to treat rotator cuff tears as soon as possible since the integrity of the tendon will not change considerably.

Acknowledgements: Support from the Department of Orthopaedic Surgery, the Department of Bioengineering

References: [1] Yamaguchi K et al. J Bone Joint Surg Am. 2006; 88-A(8):1699-1704.
[2] Gomoll AH et al. Arthritis Rheum. 2006; 50(12):3751-61 [3] Oh JH et al. Am J Sports Med. 2010; 38(4):672-678.[4] Matthews TJ et al. J Bone Joint Surg Br. 2006; 88(4):489-95. [5] Miller, RM et al. 2014. J Orthop Res. 32(10):1283-9. [6] DeOrio and Cofield. J Bone Join Surg Am. 1984;66-A(4):563-7

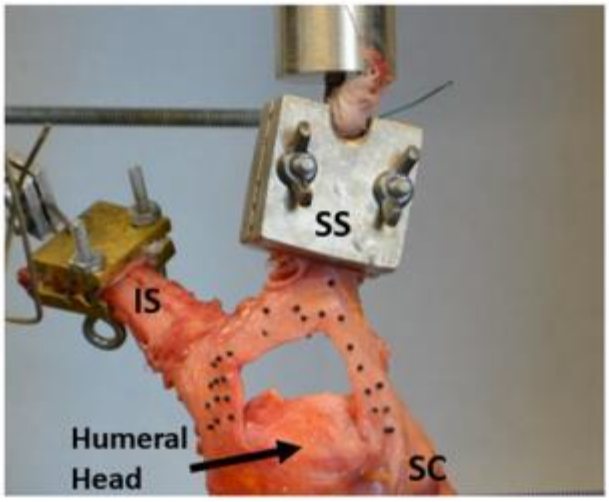

Figure 1: Test setup to simulate tensile loading at 90° coronal-plane abduction. The supraspinatus (SS) is secured to the crosshead of the materials testing machine. 22N is statically loaded to the infraspinatus (IS) via a pulley system, while the subscapularis (SC) remains unloaded.

	GROUP 1 Small/Medium < 3 cm (n = 3)	GROUP 2 Large 3 – 5 cm (n = 1)	GROUP 3 Massive > 5 cm (n = 1)
AP Tear Size at 90° abduction (cm)	1.58 ± 0.38	3.10	4.35
ML Retraction at 90° abduction (cm)	1.67 ± 0.63	3.41	5.95
Distance to LHBT at 90° abduction (cm)	5.40 ± 0.96	1.50	N/A (Past LHBT)
Stiffness at 300N (N/m)	90.7 ± 38.7	83.8	53.7
Load at Critical Tear Retraction (N)	417 ± 104	450	300

Table 1: Anatomical measurements and tensile properties for small/medium, large and massive chronic tendon tears examined.

Effects of Anterolateral Capsular Injury and Extra-Articular Tenodesis on Knee Kinematics During Physical Examination

Engel, B[1,3], Arilla, F[1,2], Azar, A[1,2], Guenther, D[1,2], Yacuzzi, C[1,2], Fu, F[2], Debski, RE[1,3], Musahl, V[1,2,3]

1. Orthopaedic Robotics Laboratory, University of Pittsburgh, Pittsburgh, PA, United States.
2. Department of Orthopaedic Surgery, University of Pittsburgh, Pittsburgh, PA, United States.
3. Department of Bioengineering, University of Pittsburgh, Pittsburgh, PA, United States.

Introduction: Interest in the anterolateral capsule of the knee has increased after the attention to rotatory stability and double bundle reconstruction of the anterior cruciate ligament (ACL) that has emerged over the past decade [1]. Recent studies suggest that procedures such as extra articular tenodesis may help to restore rotational stability[1]. However, the contribution of the anterolateral capsule combined with reconstructive procedures to knee stability are poorly understood. The aim of the present study was to evaluate kinematics in response to several clinical exams to determine the effect of anterolateral capsule injury and extra-articular tenodesis on the intact, ACL-deficient, and ACL-reconstructed knees. Our hypothesis was that the extra articular tenodesis associated with ACL-reconstruction would be necessary to reestablish intact knee kinematics when an anterolateral capsule injury associated with an ACL tear is present.

Material and methods: Seven knees from whole lower extremity fresh-frozen human cadavers (mean age 60 years) were utilized in the study. Specimens were stored at -20°C and thawed at room temperature for 48 hours before testing. A single experienced surgeon performed several clinical exams on each knee: 1) pivot shift tests based on a standardized pivot shift maneuver described by Musahl et al. [2, 3] and 2) maximal anterior load and maximal rotatory tests (internal and external rotations) of the knee at 0°, 30°, 60° and 90° of flexion. Three trials of each examination were recorded in seven knee states (Table 1). Injury to the anterolateral capsule was created by making a 2 cm incision at the level of the joint line starting 5 mm anterior to lateral collateral ligament. Extra articular tenodesis was performed by a modified Lemaire procedure . [5].

An electromagnetic tracking system (Nest of Birds, Ascension Technology) was used to measure the kinematics of the knee. Sensors were fixed to the femoral and tibial shafts utilizing titanium pins to track their motion. A stylus attached to a third sensor was used to digitize bony landmarks to establish the tibial and femoral coordinate systems used in the Grood-Suntay joint coordinate system [4]. The tracking system has a positional accuracy of 0.5 mm and an orientation accuracy of 0.5 degrees. Thus, the six degrees of freedom kinematics of the tibia with respect to the femur was determined and the primary outcome parameters were anterior tibial translation and internal/external rotation.

Multiple univariate repeated measures ANOVAs and post-hoc analysis were used to investigate differences in anterior tibial translation during the pivot shift test between knee states and to investigate differences of anterior tibial translation and internal-external rotation between knee states and degrees of flexion during the manual tests. Statistical significance was set as $P< 0.05$.

Results: *Pivot shift test*: With an intact capsule, the ACL deficient knee showed higher anterior tibial translation compared to the ACL reconstructed knee or the intact knee ($p<0.05$), however no significant difference was observed between intact, ACL reconstructed and ACL reconstructed + extra articular tenodesis knees.

Injuring the anterolateral capsule significantly increased the anterior tibial translation of ACL-deficient knee (increase of 25%, $p<0.05$). A significant decrease in anterior tibial translation was observed after ACL-reconstruction (54%, $p<0.05$) and an additional extra articular tenodesis did not result in a significant decrease in anterior tibial translation.

Manual tests: Creating an injury to the anterolateral capsule in an ACL deficient knee, a significant difference in only anterior tibial translation was found at 0˚ and 30˚ of flexion. ($p<0.05$) Following ACL reconstruction and extra articular tenodesis, no significance differences in translation or rotation for the maximum anterior and rotatory tests, respectively, were found. ($p>0.05$)

Discussion: This study examined the effect of anterolateral capsular injury and extra articular tenodesis during several clinical exams. A tear in the lateral capsule did not result in significant increases in internal rotation at all knee flexion angles. Increases in anterior tibial translation were only found at 0˚ and 30˚ of flexion. These findings partially agree with the biomechanical study from Monaco et al. [6] who found a significant difference at all degrees of flexion for anterior tibial translation after injuring the lateral capsule, and only at 30˚ for internal rotation. These differences could be explained by the capsular injury model utilized in each study. A horizontal 2 cm tear at the joint line may not represent the in vivo injury that occurs during ACL injury. In the future, an injury model to properly simulate capsular stretching will be developed to properly assess the role of this injury.

Our data also showed that an extra articular tenodesis would not be needed following ACL reconstruction since the findings from the pivot shift test were similar in the ACL reconstructed and ACL-reconstructed+tenodesis states. In addition, when ACL-deficiency was combined with a lateral capsule tear, there was no significant difference when comparing the isolated ACL-reconstruction and the ACL-reconstruction added to an extra articular tenodesis. Therefore, caution must be taken before using an extra articular tenodesis combined with an ACL reconstruction. Little evidence exists to support that it will restore intact knee kinematics. From the data in this study, extra articular tenodesis is unnecessary in isolated ACL injury. Furthermore, in the isolated ACL injury the potential to over-constrain the lateral compartment of the knee could exist with this procedure. Therefore, extra articular tenodesis should only be considered if true lateral capsular injury can be identified.

References:

1. Duthon, V.B., et al., *ACL reconstruction and extra-articular tenodesis.* Clin Sports Med, 2013. **32**(1): p. 141-53.
2. Hoshino, Y., et al., *Standardized pivot shift test improves measurement accuracy.* Knee Surg Sports Traumatol Arthrosc, 2012. **20**(4): p. 732-6.
3. Musahl, V., et al., *The pivot shift: a global user guide.* Knee Surg Sports Traumatol Arthrosc, 2012. **20**(4): p. 724-31.
4. Grood, E.S. and W.J. Suntay, *A joint coordinate system for the clinical description of three-dimensional motions: application to the knee.* J Biomech Eng, 1983. **105**(2): p. 136-44.
5. Crhistel et al., Anterio-lateral extra-articular tenodesis of the knee using a short strip of fascia lata, 2002 Sep;88(5):508-13
6. Monaco, E., et al., *Navigated knee kinematics after cutting of the ACL and its secondary restraint.* Knee Surg Sports Traumatol Arthrosc, 2012. **20**(5): p. 870-7.

Table 1: Test protocol. (ACL-R: ACL reconstructed, EAT: extra articular tenodesis)

Protocol		Data acquired
Structure injured	Procedure performed	
None	None	Intact knee Kinematics
ACL	None	ACL-Deficient knee Kinematics
ACL	ACL-R	ACL-R knee Kinematics
ACL	ACL-R + EAT	ACL-R + ITB T. knee Kinematics
ACL + Lateral Capsule	None	ACL-Deficient + Lateral Capsule deficient knee Kinematics
ACL + Lateral Capsule	ACL-R	ACL-R knee Kinematics
ACL + Lateral Capsule	ACL-R + EAT	ACL-R + ITB T. knee Kinematics

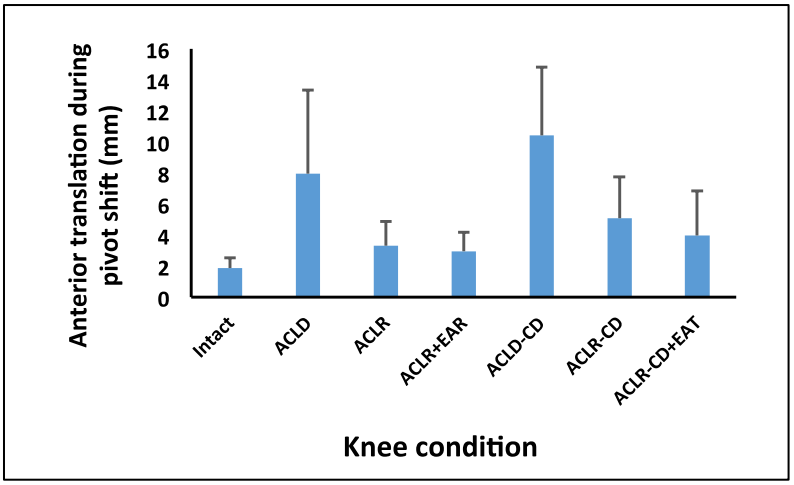

Figure1: Anterior tibial translation during the pivot shift test in seven knee states.

A New Method for Determining Cross-Sectional Shape and Area of Soft Tissues Using 3D Laser Scanning

Michaeli, Y[1, 3]; Debski, RE[1, 2]

1. Department of Bioengineering, University of Pittsburgh, Pittsburgh, PA, United States.
2. Department of Orthopaedic Surgery, University of Pittsburgh, Pittsburgh, PA, United States.
3. Department of Mechanical Engineering, ORT Braude College of Engineering, Karmiel, Israel.

Introduction: An accurate measurement of the cross-sectional area is required for evaluation of the mechanical properties of any soft tissue. Tissue contractions can cause complex geometries and deformations within soft tissues, and pose difficulties when measuring cross-sectional areas [1, 2]. Techniques developed to measure the cross-sectional area are separated into either contact or noncontact methods. Contact methods create known errors either by forcing the tissue into a geometric shape using pressure, or by assuming geometric cross-sections [4]. The objective of this study was to design and validate a non-contact device to measure the cross-sectional shape and area of soft tissues. The design constraints were 3% accuracy and 3% repeatability while using a low cost system. In addition the noncontact method needed to be simple to carry out, require minimum time, and be able to determine the cross-sectional area of multiple soft tissue types and sizes.

Methods: A non-contact method for determining soft tissue cross-sectional area was developed and validated. It was then used to determine the cross-sectional areas of in vitro porcine ACL and human MCL.

The noncontact method relies on the NextEngine® 3D laser scanner (NextEngine, Inc., Santa Monica, CA).The technology uses MultiStripe Laser Triangulation (MLT) with its array of solid state lasers to create a 3D model. The NextEngine® system is composed of a laser scanner and the AutoDrive, a rotary servo positioner, auto-incremented under scanner control. The NextEngine® 3D has been previously validated for automated and rapid calculation of cross-sectional area of long bone diaphyses [3].

To examine a specimen, it is first clamped to the AutoDrive, then the laser scan is initiated (fig. 1). After the 3D image is created, it is imported as an STL to Geomagic Verify Viewer software that is used to calculate the cross-sectional area of the specimen. The process typically takes approximately 6.5 minutes, and displays graphical results. The NextEngine® system is controlled using two parameters, (1) number of rotation increments to complete a 360° scan (4-16 increments), and (2) resolution of the scan which is determined by the laser scanning speed (speed levels 1-9).

Accuracy and repeatability of the NextEngine® system was determined by using five objects of known cross-sectional areas: 2 cylinders with known concavities (121.4, 471.1mm^2), a cuboid (163.2mm$^{2)}$, a triangular prism (212mm^2) and a cylinder with a square keyway (115.3mm^2) (Delrin, Dupont, Inc., Wilmington, DE). To minimize scanning time while maximizing accuracy, an optimized combination of rotation increments and scanning speed was determined. The first object was scanned forty eight (48) times and the Geomagic Verify Viewer calculated the area at a constant cross-section on the object. Control parameters were tested using combinations of 6, 7 and 8 rotation increments and speed levels 1-7. To further optimize scan time, the subsequent four objects were measured using 42 scans. Not all combinations were tested in these ranges and each combination was repeated three times (first object was tested

using 16 combinations and 14 combinations for the other four objects).
After the system was optimized and validated using standardized shapes, it was then used to measure human MCL and porcine ACL tissues. The ligaments were clamped to the AutoDrive and minimal tension was applied. An additional test was performed on the ACL to verify that the laser beams did not penetrate the tissue surface. The ACL was stained with India ink and the cross-sectional area was remeasured. Six scans were taken before and after staining (12 scans overall) the ACL. Six scans were taken on the human MCL and two different locations were measured on each scan. The samples were sprayed with saline to prevent dehydration.

Results: System optimization trials yielded maximum accuracy and repeatability with minimum scanning time at speed level 1 and 7 rotation increments. The NextEngine® system was able to determine the cross-sectional area and detect concavities of the standardized geometric objects (fig. 3). The mean accuracy of four objects was 2.0%. The fifth object (cylinder with a square keyway) was excluded due to cross-sectional shape that does not demonstrate a typical concavity of soft tissues. The repeatability of the laser scans was 0.5mm^2 and was not affected by the range of the object size (16.5-91.7mm^2). For human MCL at two locations, cross sectional area was 16.5±0.3mm^2 and 37.1±0.5mm^2. For porcine ACL, cross-sectional area was 91.1±0.6mm^2 and 91.7±2.2mm^2 after staining India ink on the tissue (fig. 4).The accuracy of the system is 2.0% for standardized shapes and repeatability of 1.82% for soft tissues.

Discussion: This study introduces a novel method for the determination of cross-sectional shape and area of soft tissues using laser scan data. This method produces an accurate and rapid production of a 3D image. Advantages of this method include automation, control over section orientation and the ability to examine multiple section locations across a soft tissue sample. Moreover, 3D images can be used to create 3D printed samples for future studies. For further examination of the system, testing range of sizes and types of tissues is recommended. NextEngine 3D laser scanner had met most of the design constraints as an accurate and affordable lab device (less than $5k and overall $6k including PC and clamping jig shown in fig. 2). Previous studies [1, 2] using non-contact laser systems determined cross-sectional areas within 1-5 minutes. Our goal was to similarly measure cross-sectional area within this same time interval. However, previous systems only measured the cross-section at a single location; the laser telemetric system and the laser reflectance system return the cross-sectional area as a function of its position along the axis of the object. Our system determined the cross-sectional area of the entire 3D model in 6.5 minutes.

Significance: This study establishes a new method and the use of a laser scan protocol for the automated and rapid calculation of cross-sectional shape and area of soft tissues. It provides highly accurate results that can be compared to other methods. The results of this study show that the NextEngine® overcomes the complex issue of semitransparent surfaces by not penetrating the surface and thus not underestimating the cross-sectional area. This is a low cost system that has a quick technique and simple to carry out for determining the cross-sectional shape and area of soft tissues.

Acknowledgements: Support from the Department of Orthopaedic Surgery, the Department of Bioengineering.

References:

1. Lee, T.Q., Woo, S.L.-Y., 1988. A new method for determining cross-sectional shape and area of soft tissues. J. Biomech., 110(2), 110-114.

2. Moon, D.K., Abramowitch, S. D., and Woo, S. L., 2006. The development and validation of a charge-coupled device laser reflectance system to measure the complex cross-sectional shape and area of soft tissues. J. Biomech., 39(16), 3071-3075.
3. Davies, T.G., Shaw, C.N., Stock J.T., 2012. A test of a new method and software for the rapid estimation of cross-sectional geometric properties of long bone diaphysis from 3D laser surface scans. Archaeol Antropol Sci, 4: 277-290.
4. Woo, Lee, Abramowitch, Gilbert, 2005. Structure and Function of ligaments and tendons. Lippincott Williams & Wilkins Publishing, Philadelphia, 7: 304-306.

Figure 1: Porcine ACL clamped on the AutoDrive when initiating laser scanning.

Figure 2: Clamping device designed for NextEngine® 3D laser scanner.

Figure 3: Comparison of scanned standardized shape cross-sections with reference measurements.

Figure 4: Cross-sectional measurements of porcine ACL and human MCL.

Fig 1

Fig 3

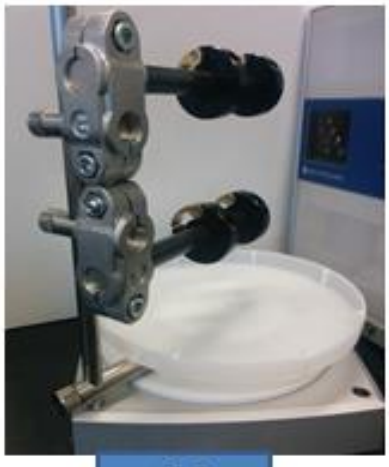

Fig 2

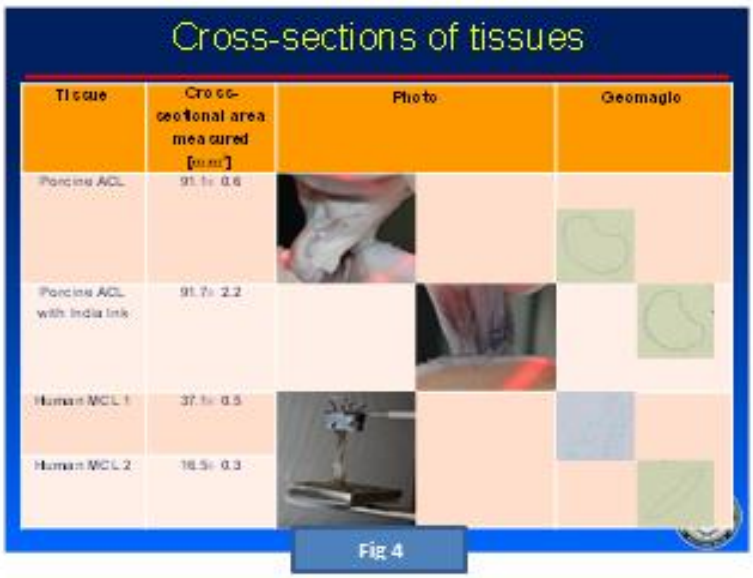

Fig 4

The Effects of Various Loading Conditions on a 3D Virtual Cervical Spine

Moss, R; Bell, KM

Department of Bioengineering, University of Pittsburgh, Pittsburgh, PA, United States.

Introduction: In vitro biomechanical testing is important in determining proper surgical techniques. Traditional testing methodologies are designed for comparative testing and have little input from in vivo data. Two separate studies have attempted to make in vitro biomechanical testing more accurately represent physiologic data by applying different loading conditions than an unconstrained pure moment, which is the current gold standard [1,2]. A study in 2013 by Dr.Bell expanded the standard pure moment loading by combining it with axial loading and follower loading [3]. This study focuses on the same loading conditions, but applying them to a 3D virtual cervical spine model and the resulting kinematics.

Methods: CT scans of fresh-frozen human cervical cadaveric specimens were created and segmented in Mimics (Materialise, Leuven) and masks were created of each of the vertebrae. These masks were then smooth and reconstructed into 3D models. The models were then exported in STL format and imported into Simulink (Mathworks Inc. MA). Ligaments were implemented in the model as listed in a study by Ahn in 2005 [4]. A spherical joint was used to model the intervertebral disc with a different stiffness for each degree of freedom. A moment of 2 Nm was applied to the top vertebrae and the resulting range of motion (in degrees) was recorded. As seen in Figure 1, there structure of the model appears as a cervical spine should, with proper spacing between each body. In the leftmost image, the attachment points for each of the ligaments is visualized with a tiny sphere. Secondly a 150 N axially compressive load was applied to the top vertebrae down through the center of rotation and the model was ran a second. Two more scenarios were ran, one with the 150 N load 5 mm anteriorly from the original position and another with the 150 N load 5 mm posteriorly from the original position.

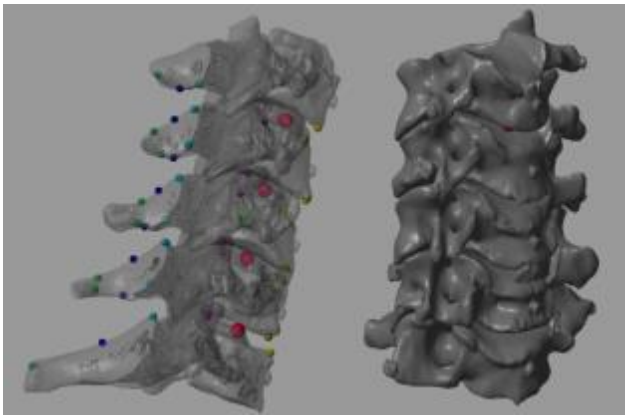

Figure 1: (Left) Partial opacity lateral photo of the model with markers for each of the ligaments (Right) Isometric view of the model

Results: The model showed between 1 and 2 degrees of motion for the C3-C4 joint and the C4-C5 joint. Between the 5-6 disc joint and the 6-7 disc joint there was an angular change between 5 and 6 degrees. Applying the compressive loading along the axis of rotation added less than a degree of rotation for each of the joints. Shifting the compressive loading 5 mm anteriorly increased the range of motion between 0.5 and 1 degrees while shifting the compressive loading 5 mm posteriorly decreased the range of motion between 0.5 and 1 degrees.

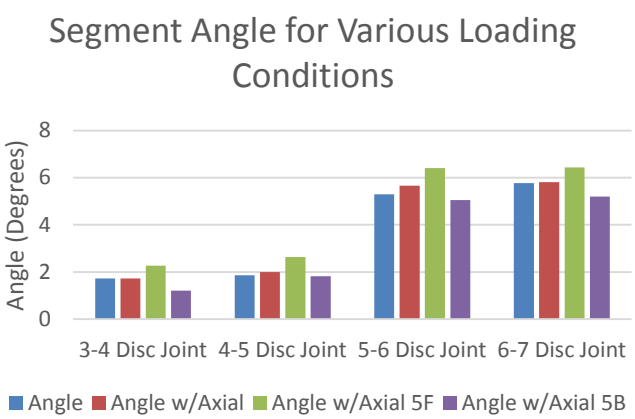

Figure 2: Graph of my data from initial testing of the model with 2 NM of torque and 150 N of compressive loading

Discussion: The structure of the model is completed, but there is still refinement of the model to finish. I believe that the reason the C5-C6 joint and the C6-C7 joint rotate more than the C3-C4 and the C4-C5 joints is that the ligaments within the upper joints have a stiffness that is generally lower than from the other two joints. The study by Dr.Yoganandan [5] has the same stiffness for the bottom two joints, and the same for the top two joints. This explains why there is similarity within each of those two groups, but differences between the two from each other. More work is still needed to finalize the model and to test the accuracy of it. However, I believe that the model will be comparable to the studies by Dr.Miura, Dr.DiAngelo, and Dr.Bell. This will allow for analysis of the different loading conditions that were applied in each of the studies. The future goal is to make the model comparable to in vivo kinematics, allowing more in-depth studies of the different medical procedures that help to reduce cervical spine degeneration such as cervical spine fusion. Overall, the model will help us to understand the forces acting on the human cervical spine, which will lead to better medical devices and procedures.

References:

[1] Miura et al., 2002
[2] DiAngelo and Foley, 2004
[3] Bell 2013
[4] Ahn 2005
[5] Yoganandan et al 2000